communications materials

Article

https://doi.org/10.1038/s43246-024-00492-6

Martensite decomposition during rapid heating of Ti-6Al-4V studied via in situ synchrotron X-ray diffraction

Check for updates

Seunghee A. Oh [1,4] ✉, Joseph W. Aroh[1], Nicholas L. Lamprinakos [1], Chihpin Andrew Chuang [2], Ashley N. Bucsek [3] & Anthony D. Rollett [1] ✉

Martensite, α‘, commonly appears in Ti-6Al-4V upon rapid cooling from above the β-transus temperature. It is known that α‘ decomposes into α and β at high temperatures but well below the β-transus temperature. Here, we study the decomposition of martensitic Ti-6Al-4V under rapid laser heating, employing in situ synchrotron X-ray diffraction. A comparison is made with post-annealed Ti-6Al-4V under heating to elucidate changes without martensite decomposition. The fast acquisition of X-ray diffraction data at 250 Hz temporally resolves the decomposition process initiated by annihilating dislocations in α‘. The recovery process is accompanied by structural changes in martensite, followed by the phase transformation to β. Thermal profiles estimated from the lattice parameter data reveal the influence of heating rates and dislocation densities on the decomposition process. Throughout the analysis of the diffraction profiles with respect to estimated temperature, we propose a straightforward method for approximating the initiation temperature of martensite decomposition.

Titanium alloys are renowned for their exceptional mechanical properties, corrosion resistance, and biocompatibility, making them widely used in various applications. For Ti-6Al-4V, one of the most popular α + β titanium alloys, a wide range of microstructures and properties can be achieved based on variations in processing[1–6].

The metastable phase, martensite α’, is commonly observed in the Ti-6Al-4V after processes involving high cooling rates, such as quenching, laser welding, or additive manufacturing[1,7–9]. The α’ is a distorted HCP phase that has higher vanadium and lower aluminum contents than a thermodynamically stable phase, α, as a result of the diffusionless transformation where no segregation occurs[10]. During rapid cooling from above the β-transus temperature, the high-temperature BCC phase, β, transforms into α’, which typically exhibits a fine acicular microstructure[11,12].

In martensite, a high density of dislocations and twins are generated to accommodate the shape deformation associated with the martensitic transformation[13]. The high density of dislocations contributes to the high strength of the martensitic Ti-6Al-4V, and it also causes low ductility, in part due to the absence of the ductile β phase[1,14–16]. Therefore, martensitic Ti-6Al-4V is generally considered to be less desirable for engineering applications[17,18] and there have been many studies to tailor the microstructure by decomposition of the martensite, known as tempering[5,16,19–23].

Martensite decomposition corresponds to the transformation of the metastable α’ to a mixture of thermodynamically stable α and β phases by annealing the martensitic Ti-6Al-4V. Complete decomposition is known to be achieved at temperatures above 700 °C[5,19,23]. To enhance the performance of initially martensitic Ti-6Al-4V components, many studies have aimed to optimize the annealing process[6,8,12,16,19,20].

The detailed investigation of how the α’ lattice evolves during decomposition presents challenges as α and α’ share the same crystal structure, HCP, with similar lattice parameters, making differentiation difficult. Despite this difficulty, a few investigations have endeavored to uncover the intricacies of martensite decomposition. Some claimed that the martensite decomposition begins with the formation of the β phase and the β-stabilizer (i.e., V) depleted martensite, α'_{depl}, which subsequently transforms into α[21,24]. Furthermore, several studies have examined the role of alloying element diffusion on dislocation density and the shape and dispersity of precipitated β during the decomposition[4,16,20,25]. Recently, Wang et al.[26] discovered a β-stabilizer-rich phase, α_{HME}, through TEM analysis of

[1]Department of Materials Science and Engineering, Carnegie Mellon University, Pittsburgh, PA, USA. [2]X-ray Science Division, Advanced Photon Source, Argonne National Laboratory, Lemont, IL, USA. [3]Department of Mechanical Engineering, University of Michigan, Ann Arbor, MI, USA. [4]Present address: Department of Mechanical Engineering, University of Michigan, Ann Arbor, MI, USA. ✉e-mail: seungheo@umich.edu; rollett@andrew.cmu.edu

an as-printed Ti64 block, suggesting it as an intermediate phase preceding the formation of the β phase during martensite decomposition[26].

In addition to the ex situ studies, a few previous in situ studies have examined martensite decomposition. Brown et al.[27] used in situ synchrotron X-ray diffraction during continuous heating of as-printed Ti-6Al-4V. Through analysis of continuously collected diffraction profiles and diffraction line profile analysis (DLPA), they found the critical temperature associated with the recovery of dislocations in the as-printed part under continuous heating at a rate of 100 K/min. However, most other in situ reports only provide limited information from isothermal experiments or rely on indirect evidence[7,12,28,29], potentially leading to misinterpretations of the decomposition process. Ascertaining the fundamental details of the decomposition process remains a challenge and necessitates advanced experiments.

Transmission electron microscopy (TEM) and X-ray diffraction are commonly employed techniques to characterize martensite decomposition. TEM allows for the direct examination of compositional variations and dislocation structures, particularly at the microscale level, making it suitable for studying martensite and its decomposition[6,22,26,30]. X-ray diffraction is a non-destructive technique ideal for investigating continuously changing behaviors. In particular, the width of the diffraction profiles is sensitive to microstrain induced by internal stress from defects within a grain and crystal size. Consequently, X-ray diffraction has been used extensively to study the evolution of defects, i.e., dislocations, and crystal size in martensite[12,23,25,27,31–34].

This study presents a time-resolved investigation of martensitic decomposition via in situ synchrotron X-ray diffraction, focused on laser-induced rapid heating. The high temporal resolution (250 Hz) of the X-ray diffraction setup allows for the observation of rapid behaviors involved in the martensite decomposition process in Ti-6Al-4V. The synchrotron X-ray diffraction setup used in the study has microscale spatial resolution, allowing precise measurements of heated regions. However, due to the limited number of grains in the measured area, quantitative analyses such as DLPA are not appropriate. Nonetheless, by excluding a few factors affecting the measured diffraction profiles, examination of the continuously changing profiles enables quantitative analysis of the martensite decomposition process. Specifically, the rapid heating rates ranging from 10^3 to 10^4 K/s were expected to mitigate the effects of grain growth and recrystallization on the widths of the diffraction profiles.

The measurements of martensite decomposition were achieved by probing the heat-affected zone (HAZ) below a laser weld in a sample cut from an additively manufactured Ti-6Al-4V block. A control sample with fully decomposed martensite (i.e., α + β), was prepared by annealing the same as-printed Ti-6Al-4V at 800 °C for 2 h. This study's comparison between the two Ti-6Al-4V samples that differed in the presence/absence of martensite, provides new evidence for characterizing the martensite decomposition from the continuously acquired X-ray diffraction profiles. In addition, the direct observation of martensite decomposition at different heating rates reveals how diffusion affects the crystal structure and dislocation densities in the lattices of martensitic Ti-6Al-4V during rapid heating.

Results

Materials: as-printed Ti-6Al-4V and post-annealed Ti-6Al-4V

The backscattered electron (BSE) images in Fig. 1a, b present general phase configurations of the base metals, the as-printed Ti-6Al-4V and the heat-treated Ti-6Al-4V, which were used in the heating experiments. The marginal contrast difference observed in the as-printed Ti-6Al-4V indicates an almost single-phase microstructure, which is assumed to be mostly acicular α'. Such a microstructure is well-known to be characteristic of martensitic Ti-6Al-4V[8,28]. In the post-annealed Ti-6Al-4V (Fig. 1b), the overall microstructure is characterized by bright and dark regions, corresponding to the β and α phases, respectively. Therefore, it can be inferred that the martensite largely decomposes into an α + β microstructure through annealing at

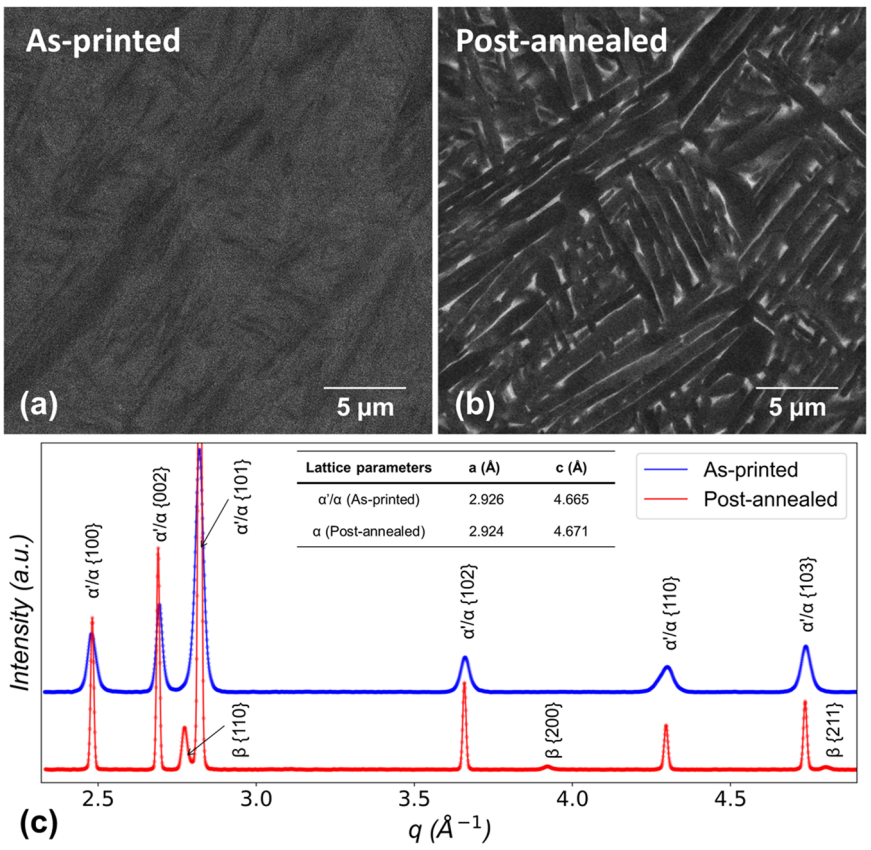

Fig. 1 | Prepared Ti-6Al-4V specimens. BSE-SEM images showing the cross-sections of (**a**) as-printed Ti-6Al-4V and **b** post-annealed Ti-6Al-4V, and **c** their azimuthally integrated diffraction profiles (intensity-q (Å^{-1})).

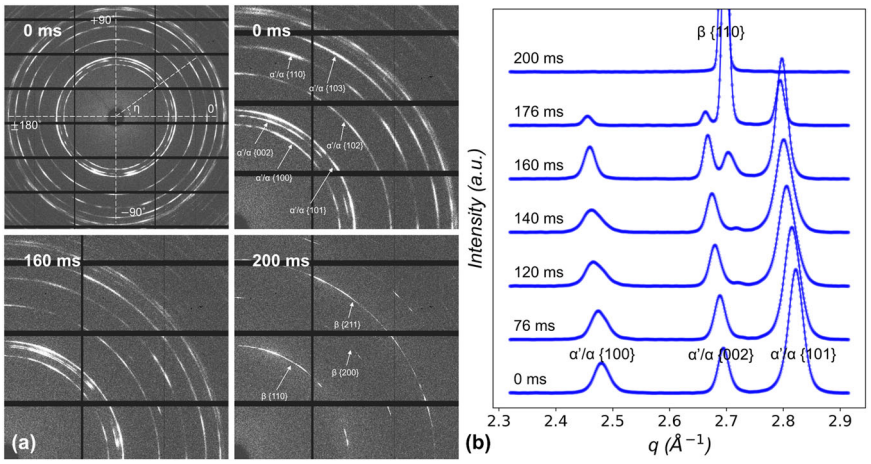

Fig. 2 | Evolution of diffraction data of as-printed Ti-6Al-4V during the heating experiment. a Two-dimensional diffraction patterns and **b** one-dimensional (intensity-q) profiles.

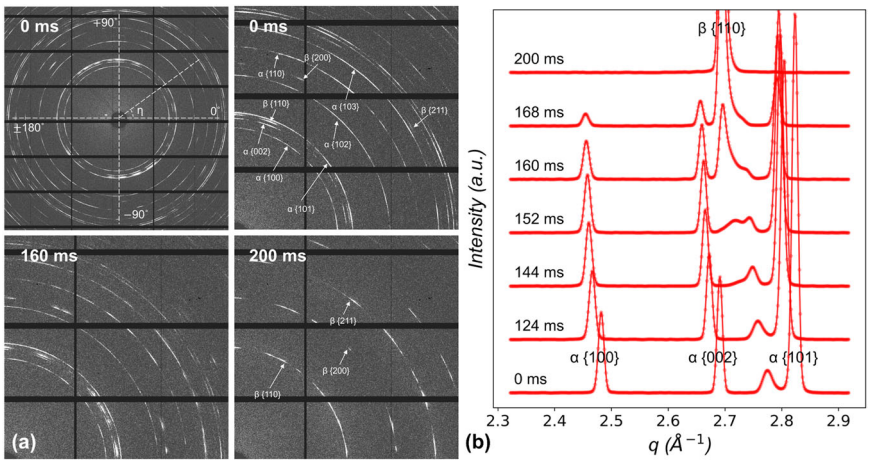

Fig. 3 | Evolution of diffraction data of post-annealed Ti-6Al-4V during the heating experiment. a Two-dimensional diffraction patterns and **b** one-dimensional (intensity-q) profiles.

800 °C[23]. This observation is consistent with the integrated diffraction profiles (intensity-q (Å^{-1})) in Fig. 1c where the strong peak of β {110} appears between α'/α{002} and α'/α{101} in the post-annealed sample, while no β profile is detected in the as-printed Ti-6Al-4V. Furthermore, the diffraction profiles reveal that the peak width decreases in the annealed Ti-6Al-4V compared to the as-printed sample, indicating significant changes in the microstrain and crystallite size of the hexagonal phase after post-annealing. The peak positions (q) of the HCP phases are comparable in both samples, but the {002} of the annealed sample is positioned at slightly lower q than that of the as-printed sample, suggesting accompanying changes in the anisotropy of the crystal structure as the martensite decomposes.

Phase evolutions during laser heating

Figures 2 and 3 show the evolution of the diffraction data at different time stamps during the heating experiments conducted at 25 W power and 5 mm/s velocity of a laser scan. The images at 0 ms in Figs. 2a and 3a are the acquired diffraction patterns of the unheated samples. In both images, the intensity distributions of the diffraction rings are uneven, and the {002} rings are intermittent around the azimuth. These features possibly indicate that the microstructure is textured, commonly observed in printed Ti-6Al-4V. However, the diffraction rings of lattice planes with larger multiplicities in the hexagonal system appear continuous, suggesting that it also has a fine microstructure with many grains even within the small measured volumes (≈50 × 30 × 400 μm^3). For the quantitative analysis interpretations, the 2D diffraction patterns are azimuthally integrated to convert them into 1D profiles (Figs. 2b and 3b). The general characteristics, including thickness and radius, of the rings in 2D images correspond to the shape and q position of peaks in 1D profiles. The reference time, 0 milliseconds (ms), is defined as the time at the beginning of the laser heating process.

In Fig. 3b, the {110} profile of the transformed β appears at a lower q value than the {110} profile of the pre-existing β between 152 and 160 ms. This finding matches the 2D patterns in Fig. 3a at 160 ms where the β{110} line is wider than that before heating. It is evident that the peak positions, corresponding to the lattice parameters, for the transformed β and pre-existing β are different, suggesting compositional differences between them. This difference is attributed to the higher vanadium (V) content in the pre-existing β lattice, which partitioned to the β as the martensite slowly decomposed to the thermodynamically stable form during annealing, thus leading to a decrease in the BCC lattice parameter[10,26,35]. The vanadium concentration in the β lattice subsequently becomes smaller and more homogeneous as the alloying elements redistribute between the two types of β during the phase transformation under rapid heating.

In Fig. 2a at 0 ms, no clear β peak is present before heating, indicating a predominantly martensitic sample. However, a hazy region located between {002} and {101} rings suggests that the β may exist at very small fractions in the sample. A discernible peak emerges at 120 ms, but its intensity remains unchanged by 140 ms. Therefore, this behavior does not signify the initiation of the phase transformation to β at 120 ms. The cause remains unclear, but it is plausible that the orientations of the pre-existing β grains in the as-printed Ti-6Al-4V were influenced by neighboring grains during continuous laser heating, resulting in diffracted beams falling on the detector. The presence of this small β peak enables us to analyze the evolution of the β lattice in the as-printed Ti-6Al-4V before the phase transformation during heating and to compare it with the corresponding results from the annealed Ti-6Al-4V, as shown in Fig. 4.

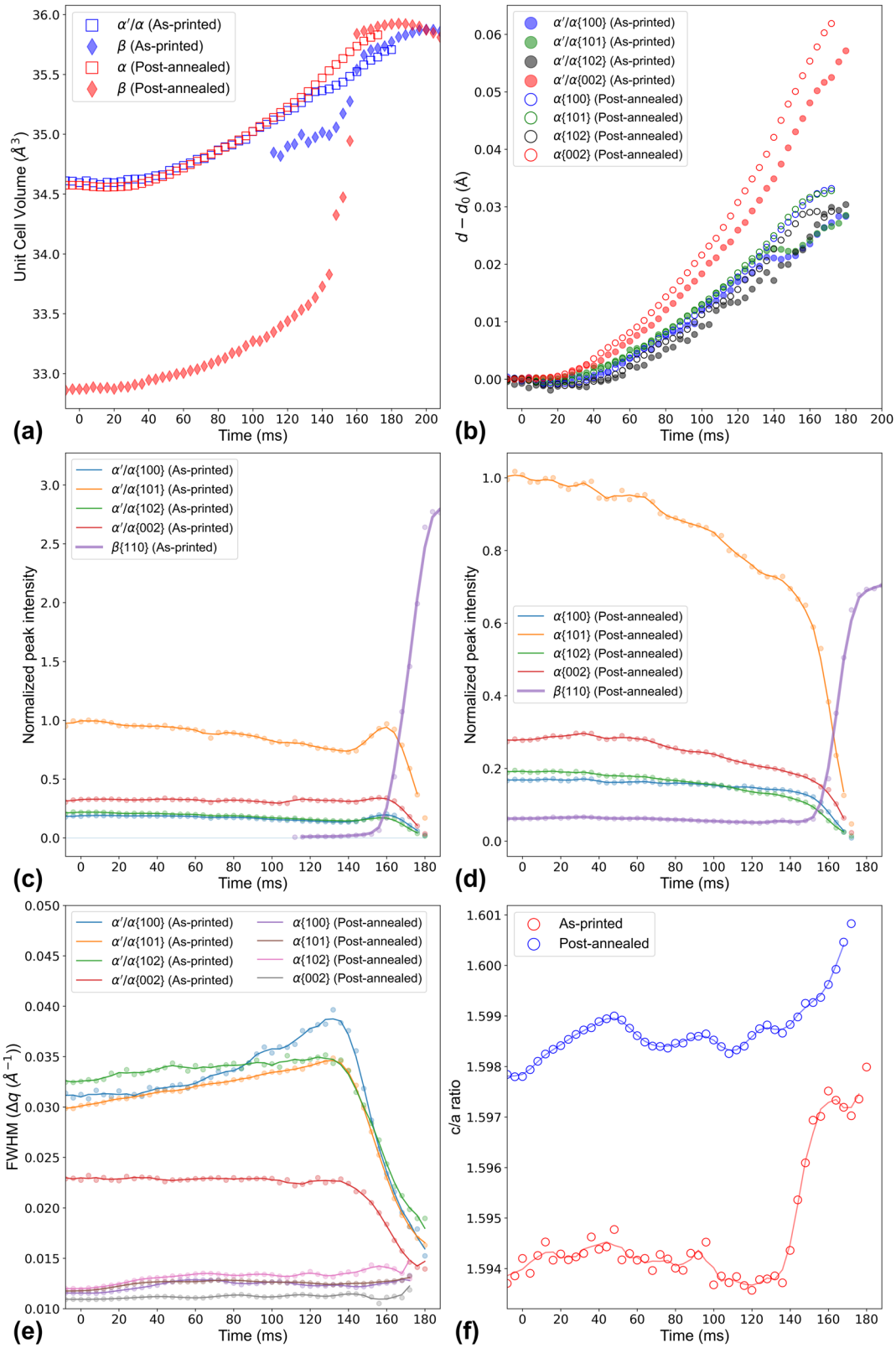

Fig. 4 | Evolution of diffraction profiles of the as-printed and post-annealed Ti-6Al-4V during the heating experiments. a The unit cell volumes of α'/α and β, **b** the changes in the lattice spacing of α'/α, **c** the normalized peak intensities of α'/α and β by the initial intensity of α'/α{101} in the as-printed Ti-6Al-4V, **d** in the post-annealed Ti-6Al-4V, **e** the FWHM, and **f** the c/a ratio of the hexagonal phases with moving average trendlines.

Time-resolved investigations of diffraction profiles during laser heating

As depicted in Fig. 4a, the hexagonal phases in the two samples exhibit only marginal differences in unit cell volume. However, from 136 ms until the phase transformation to the β terminates, the unit cell volume of the hexagonal lattice in the as-printed Ti-6Al-4V remains noticeably smaller than in the annealed Ti-6Al-4V. This divergence indicates that a structural change starts in the α' lattice from 136 ms, resulting in a distinct hexagonal

Table 1 | List of experiments with different laser parameters using as-printed Ti-6Al-4V and corresponding heating rates calculated from the estimated temperatures

ID	Power	Velocity	Heating rate
LH-S2	25 W	2 mm/s	3200 K/s
LH-S1	25 W	3 mm/s	5100 K/s
LH-0	25 W	5 mm/s	8500 K/s
LH-F1	40 W	5 mm/s	10,500 K/s
LH-F2	55 W	5 mm/s	14,000 K/s

lattice of the as-printed Ti-6Al-4V from the α in the annealed Ti-6Al-4V. Moreover, a significant disparity is noticed in the volume of the β lattice between the two samples, indicating a significant difference in the compositions of the β between the two samples. Nonetheless, during the onset of the phase transformation to β, the BCC lattices in both samples undergo rapid expansion until their volumes slightly surpass that of the hexagonal lattices.

Figure 4b illustrates how lattice spacing of α'/α changes over time during heating. To facilitate comparison across different lattice planes, the lattice spacings are normalized by calculating the difference between each time-resolved lattice spacing, d, and the initial spacing, d_0, before heating. The lattice spacings of {101} and {100} experience temporal arrest between 136 and 152 ms in the as-printed Ti-6Al-4V, while the {002} spacing exhibits a monotonic increase under heating. This behavior is evidenced by the rapid increase in the c/a ratio, calculated using {002} and {100}, as shown in Fig. 4f. The results suggest a sudden anisotropic change in the lattice of the as-printed Ti-6Al-4V between 136 and 152 ms. And, the exact cause for the fluctuation in the c/a ratios, commonly observed in both heating experiments, remains unclear, but it can be related to the anisotropies in the diffusivity of solutes and thermal expansion in the hexagonal lattices[36,37].

Figure 4c, d illustrates the evolution of peak intensities, normalized by the initial intensity of the {101} α'/α profile. Owing to thermal effects on the diffracted X-rays, the peak intensities in both figures gradually decrease under heating. At the onset of the phase transformation, when the β lattice rapidly expands, the amount of β gradually increases. Consequently, the rapid growth of β initiates when the lattice volumes of the two phases become similar, as shown in Fig. 4a. These results imply that high coherency between the two lattices favors the phase transformation. In addition, the overall peak intensities in the as-printed Ti-6Al-4V increase from 140 ms to 160 ms. This behavior is attributed to the rapid decrease in the Full Width Half Maximums (FWHMs), as described in Fig. 4e, since the profile areas of α'/α should remain constant before the phase transformation occurs (Figs. 5b and 6a).

Figure 4e depicts the evolution of the FWHMs of the hexagonal phase profiles over time. As shown in Fig. 2, the as-printed Ti-6Al-4V exhibits much broader peak profiles compared to the annealed Ti-6Al-4V, ascribable to a higher density of dislocations in the martensitic α' phase. Evident and sudden decreases in the FWHM simultaneously occur in all reflections of α'/α in the as-printed Ti-6Al-4V from 136 ms. This timing coincides with the abrupt increase in the c/a ratio in Fig. 4f. Although defining the exact initiation time for the phase transformation to the β phase is challenging due to the intrinsic detection limitations of the fast X-ray diffraction technique in small peaks, the discernable onset of the phase transformation is observed after the occurrence of these simultaneous changes in the α'/α. The result indicates that the temperatures at which the FWHM and c/a ratio changes occur are lower than the phase transformation temperature to β. In contrast, in the annealed Ti-6Al-4V, which is assumed to be only marginally martensitic, no noticeable changes in the profiles are observed before the phase transformation.

Discussion

For further investigations into the unidentified behaviors, four different laser heating (LH) experiments, as described in Table 1, were conducted using the as-printed Ti-6Al-4V. These experiments aimed to examine the effects of various heating rates on the diffraction profiles by altering the power and velocity of the laser scanning. The laser condition used for the as-printed and post-annealed Ti-6Al-4V, presented in Fig. 4, is labeled as LH-0.

Temperature estimations based on thermal expansion behavior were conducted for experiments with as-printed Ti-6Al-4V, as shown in Fig. 5a. These estimated temperatures are uncertain enough that the temperature range within which specific events occur can only be bracketed because, e.g., mechanical and compositional effects on lattice spacings are unknown. However, the estimation is useful for comparing similar experiments with different thermal histories on a material and provides actual in situ thermal histories on measured grains, unlike other comparative methods that either measure sample surfaces or ignore spatial thermal gradients within a bulk sample. Such methods are unsuitable for microscale in situ experiments.

Figure 5a demonstrates how the temperature of the α'/α phase changes over time for five different experiments, each reaching similar temperatures at different timings, indicating different heating rates. The errors were calculated from the standard deviations of the estimated temperatures based on lattice spacing of different lattice planes. Although the heating rates vary continuously during the experiments, the temperature-time curves in Fig. 5a are nearly linear, which permits linear fits to calculate the overall heating rates, as shown in Table 1. The experiment (LH-0) presented in Fig. 4 has a heating rate of around 8500 K/s, which is faster than LH-S1 and LH-S2 but slower than LH-F1 and LH-F2.

Accordingly, the phase transformation begins at a different time for each experiment, depending on its associated thermal history. The profile area (integrated intensities) evolutions in Fig. 5b provide quantitative information on the phases per time interval. For cross-experiment comparison, {101} profiles are exclusively presented. To minimize the thermal effects on the diffracted X-ray intensities, the Debye–Waller factors[32,38] were approximated using the estimated temperature and then applied to the profile areas. Some experiments, i.e., LH-S2 and LH-F2, exhibit gradual reduction in area over time before the phase transformation, attributed to inaccuracies arising from temperature estimations and the calculation of the thermal factor, M, on the diffraction intensity, based on $I = I_0 \cdot e^{-2M}$ where I is the observed intensity and I_0 is the intensity at rest. Regardless, the experiments consistently display rapid decreases in the profile area, representing the moment of the phase transformation to the β for each experiment. In Fig. 5c, d, the initial c/a ratios vary between experiments, similarly to the initial FWHM, both of which stem from slight local non-uniformities in the hexagonal phases (α'/α) in the as-printed Ti-6Al-4V. Nonetheless, the abrupt changes in the c/a ratio and the FWHM are consistently evident in all experiments before the phase transformation to the β. These findings clearly point to a discrete reaction occurring at a lower temperature than the phase transformation temperature in the martensitic Ti-6Al-4V.

To identify the reaction, we analyzed the profile parameters as a function of the temperature. Figure 6a presents the profile area evolution of the α'/α{101} as a function of temperature, providing temperature ranges for the phase transformation temperature from α'/α to β in each experiment. There is a consistent trend of decreasing area with rising temperature across different experiments. The phase transformation typically terminates at a lower temperature for slower heating. The phase transformation in LH-F2 appears to be complete at a lower temperature than other experiments, but this is ascribed to the small number of collected data points due to its higher heating rate. Overall, the phase transformation to the β is confirmed as a diffusional process significantly influenced by the heating rate.

Similarly, the notable change in FWHM, shown in Fig. 6b, is affected by the heating rates, indicating its association with a diffusional process. The size effects on the profile widths caused by grain growth are considered negligible owing to the rapid heating process in this work. Moreover, the consistency between the profiles obtained from the azimuthally sectioned diffraction patterns at 15° intervals in Supplementary Fig. 4 verifies that the changes in the FWHM are likely due to the changes in the intragranular strain (microstrain) during heating. Therefore, the observed result primarily stems from the rapid reduction in microstrain within the lattices

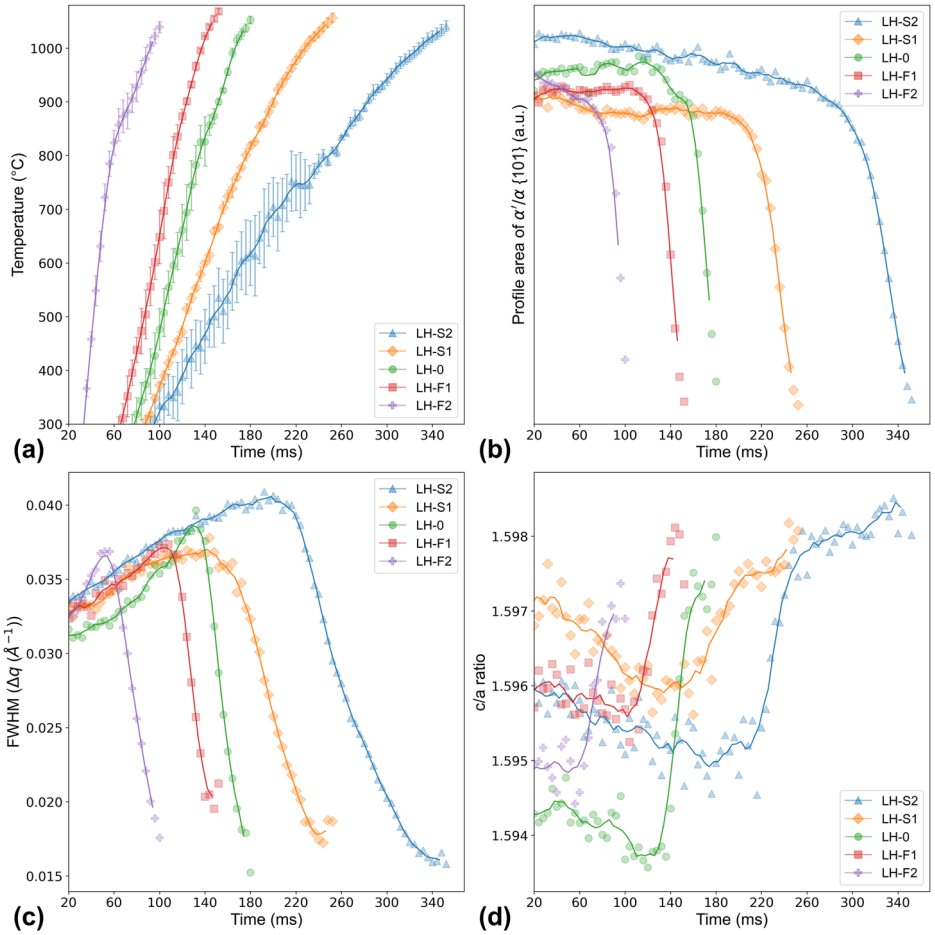

Fig. 5 | Evolution of each experiment as a function of time during the rapid heating experiments. **a** Inferred temperature, **b** peak area (α'/α{101} peak), **c** peak width (FWHM-α'/α{100}), and **d** c/a ratio.

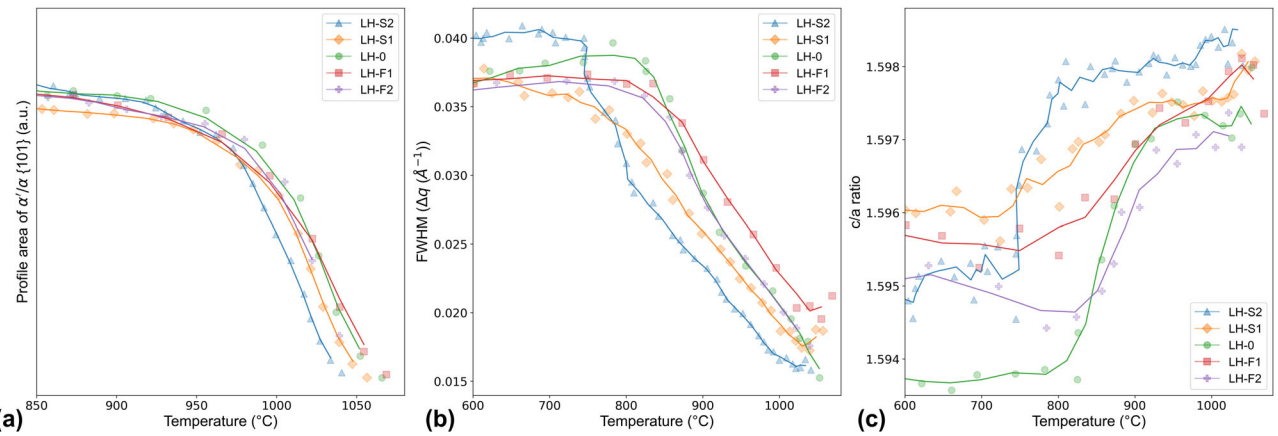

Fig. 6 | Evolution of profile parameters as a function of temperatures during the rapid heating experiments. **a** Peak area (α'/α{101} peak), **b** peak width (FWHM-α'/α{100}), and **c** c/a ratio.

corresponding to rapid decreases in dislocation density. In Fig. 6c, while the increments in the c/a ratios depend on the initial values, all experiments show an increase in the c/a ratio, which occurs simultaneously with the change in the FWHM. This suggests a clear relationship between the reduction in dislocation density in the martensite and the alteration in crystal structure.

As multiple profile parameters undergo coincidental and complex changes over a short time, the profile parameters of LH-0 shown in Fig. 4 are reexamined in Fig. 7. This presentation aims to clarify the evolving sequence of changes and is accompanied by detailed discussions for each change. Initially, during the early heating stage prior to the phase transformation, thermal expansions occur in both the β (blue marker) and α'/α (red marker) lattices at a similar rate. Subsequently, the β lattice rapidly expands from 152 ms while the growth of the β{110} peak remains marginal (green marker). This result implies that the existing β phase exchanges the alloying elements, particularly V, with the α'/α during this stage[35]. The phase transformation gains momentum as coherency between the BCC and hexagonal phases increases. Thus, the transition in the increasing lattice volume gradient of the β under heating can be deemed the pivotal point indicating the onset of the phase transformation.

In Fig. 7, it is evident that the rapid changes in the FWHM (brown marker) and c/a ratio (purple marker) of the α'/α profile begin 16 ms ahead

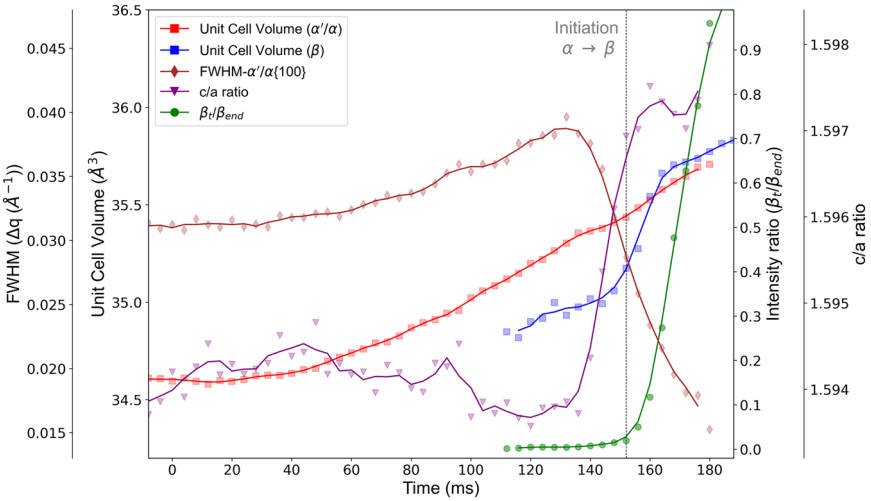

Fig. 7 | Temporally resolved examinations of behaviors in the martensitic Ti-6Al-4V during laser heating. Replotted graphs of the profile parameters of the LH-0 experiment presented in Fig. 4.

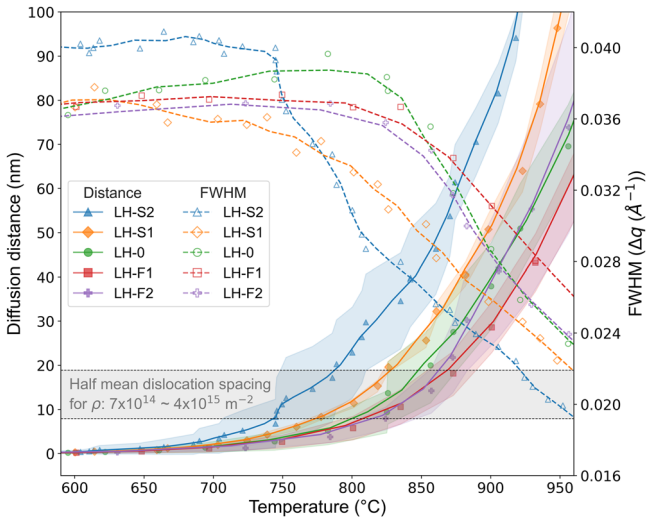

Fig. 8 | Correlations of changes in dislocation densities with diffusion behaviors in martensitic Ti-6Al-4V. Diffusion distance of V in the α'/α and FWHM of the profiles with moving average trendlines as a function of temperature during heating for the five different experiments.

of the initiation. During the stage when the dislocation density (ρ) starts to decrease, generally termed recovery, the dislocations are easily self-annihilated, resulting from canceling out of a pair of dipoles. This phenomenon arises due to the climb motion of dislocations. The motion is driven by the diffusion of point defects, including vacancies, and is thermally activated. For dislocations of opposite signs to mutually annihilate, they must traverse at least half the distance between them. The mean dislocation spacing (MDS) between dislocations can be estimated as $1/\sqrt{\rho}$ (per unit length), and it is proportional to the dislocation cell size.

In Fig. 8, the solid lines represent the diffusion distance of V in the hexagonal phase. The distances are estimated by integrating the diffusion length for each time interval, calculated using $X(t) = 2(Dt)^{1/2}$ where t is time, X is the diffusion length of an element, and D is the chemical diffusion coefficient obtained from TCTI3 and MOBTI4 databases in ThermoCalc software[39]. The standard deviations of the estimated diffusion distances from temperature profiles estimated from different lattice planes were used to represent errors, and these were plotted as shaded color regions. Vanadium diffuses faster than aluminum in the α phase, making it a preferred solute for swapping with vacancies in the solid solution phase. Assuming that the diffusion coefficient of the vacancy is comparative to that of V within the α lattice of Ti-6Al-4V, the MDS is computed based on the dislocation densities. The dislocation density in the martensite is known to range between 10^{14} and 10^{15} m^{-2} (see refs. 22,33,40). Due to the limited accuracy in quantifications using line profile analysis associated with the dataset in our experiments, which is attributed to the restricted number of grains in the measured volume, this work utilized the reported dislocation densities for as-printed Ti-6Al-4V[25,27,40].

The temperature ranges at which the calculated diffusion distances correspond to half of MDS coincide with the temperature range where the FWHM begins to decrease. Furthermore, this approach is applicable to a slower heating experiment in ref. 27 with as-printed Ti-6Al-4V. They observed a decrease in the FWHM of the diffraction profiles (α'/α) with a heating rate of 100 K/min around 497 °C, which is the highest temperature among three other experiments they conducted at the same heating rate. The result is comparable to the approximation of the dislocation spacing calculated from $\rho = (4 \pm 0.5) \times 10^{15}$ m^{-2}, which is ~431 °C. Furthermore, this approach is confirmed by another experiment in our work, shown in Supplementary Fig. 5, with a heating rate exceeding 50,000 K/s. In this experiment, the sample was heated to ~870 °C before undergoing cooling. Here, the FWHM begins to decrease when the diffusion distance of V reaches half of MDS during the process.

In Fig. 7, the FWHM steadily decreases from 136 ms until the entire hexagonal phase transforms into the BCC phase. Conversely, starting at 152 ms, the rapid increase in the c/a ratio diminishes, becoming less significant compared to the earlier changes, while the volume of the β rapidly expands. These findings suggest a scenario where dislocation annihilation occurs through two distinct reactions occurring sequentially, with a certain degree of temporal overlap.

One plausible explanation for this behavior is that while the dislocation annihilation resulting from the canceling out of dipoles completes early[32] at the initial stage of the phase transformation to β, the exchange of alloying elements between α'/α and β phases expedites dislocation annihilation by redistributing solutes between the phases[30,41]. This behavior is more evident in the slower heating experiments, LH-S1 and LH-S2. Figures 5 and 6 show that, after the rapid increase in the c/a ratio, the c/a ratio still increases over time (and temperature) with a reduced gradient. Concurrently, the FHWM consistently decreases over time, implying that the self-annihilation of the dislocation dipoles terminates early in the martensite decomposition, while the dislocation removal process persists until the phase transformation finishes.

The c/a ratio is a parameter that represents the structural anisotropy of the hexagonal crystal system, and it serves as evidence to distinguish microscopic changes in the phase. Previous studies have reported that the c/a ratio of α' is smaller than that of α in the α + β microstructure[7,8,28]. A c/a ratio closer to 1.633 implies a crystal structure closer to HCP, which is further away from martensite. Therefore, an increase in the c/a ratio along

with a reduction in the dislocation density in martensite can indicate the decomposition of α' to α. As the elastic microstrain energy in the distorted lattice is relieved, a distinct anisotropic change (c/a ratio) occurs in the martensitic lattice, resulting in the decomposition of the metastable crystal structure to a stable hexagonal structure. Even under the rapid heating process, the relaxation of dislocations in the martensite is significant.

As a result of this recovery, the lattice volume of the hexagonal phase in the as-printed Ti-6Al-4V is temporarily smaller compared to that of α in the annealed Ti-6Al-4V, appearing as a gap in in the lattice volumes between the two different Ti-6Al-4V in Fig. 4a. This is ascribed to the mitigation of distortion within the α' lattice. In addition, in accordance with the known relationship where an increase in V content in the α leads to a reduction in its lattice parameters, it is attributed to a higher V content in the distortion-relieved hexagonal phase compared to the α in the annealed sample[35,42,43]. Moreover, this state of the hexagonal phase is presumed to be the intermediate phase, α_{HME}, reported in ref. 26. Overall, several events observed in the diffraction profiles collected by the in situ measurements suggest the possibility that the decomposition of α' is initiated by relaxing the distorted lattice with the annihilation of dislocations, which produces a vanadium-rich hexagonal phase before transforming to the β phase under the rapid heating process. The results also indicate that an acicular morphology does not necessarily represent the fully martensitic microstructure[44].

Conclusion

In summary, significant changes in the diffraction profiles of α'/α are observed before the phase transformation to β occurs during continuous heating of as-printed (martensitic) Ti-6Al-4V. Utilizing a high-speed in situ X-ray diffraction system, this study effectively resolves the details of the changes, and the use of a laser source for rapid heating helps mitigate size effects on the diffraction profiles. Our findings suggest the possibility that the decomposition of α' to α + β begins as the dislocations annihilate in the α', leading to the formation of a V-rich hexagonal phase with a less distorted structure than the α', prior to the formation of the α + β microstructure. This observation supports Wang's claim[26] regarding the presence of an intermediate phase, α_{HME}, during martensite decomposition, although the changes appear too continuous to warrant classification as a separate phase. Additionally, through several experiments with varying heating rates, we discovered that the onset of the diffusional process is associated with a specific temperature range within which vacancies (or solutes) can diffuse over half of the mean dislocation spacing. The temporally resolved decomposition process in this work offers valuable insights to optimize the microstructure of the martensitic Ti-6Al-4V.

Methods

The entire samples were obtained from an as-printed Ti64 block, 60 × 60 × 8 mm^3. The block was fabricated using EOS Ti-6Al-4V Grade 5 standard powder on an EOS M 290 system. The laser scanning during the build had no rotation between each 30-μm printing layer. The key printing parameters were as follows: laser power of 280 W, scanning speed of 1200 mm/s, hatch spacing of 140 μm, and spot size of ~100 μm. A portion of the as-printed block was sectioned off to prepare a Ti-6Al-4V sample where the martensite was fully decomposed. The sectioned part was annealed with a 10 K/min heating rate at 800 °C for 2 h, followed by air cooling. Subsequently, the prepared as-printed block and annealed piece were cut into thin plates, measuring 40 × 3 × 0.4 mm^3, oriented at an angle of 67° with respect to the printing scan direction, using electrical discharge machining as illustrated in Supplementary Fig. 1. To examine the microstructures of the prepared samples, a TESCAN MIRA-3 FEG scanning electron microscope (SEM) was utilized.

The in situ experiments were conducted at the 1-ID-E beamline at the Advanced Photon Source in Argonne National Laboratory, following the same experimental setup as our previous experiments[9,11]. The monochromatic X-ray beam energy used in this work was 61.33 KeV ($\lambda \approx 0.2022$ Å), with a beam size of 50(h) × 30(v) μm^2. The X-ray beam was centered at 30 μm below the surface to observe the microstructural behavior in the HAZ below the laser track. Supplementary Fig. 2 presents a schematic of the in situ heating experimental setup. Prior to laser heating, the surfaces of the prepared samples were polished to ensure consistent laser-material coupling along the scan path. Laser scanning was performed with different laser power and velocity, as summarized in Table 1, to manipulate the heating profiles. The laser maintained a fixed spot size of 100 μm and a scan length of 2.0 mm. The Pilatus3X 2 M CdTe detector was positioned downstream of the sample at an appropriate distance, covering at least six rings of the hexagonal phases. Each diffraction image was acquired at intervals of 4 ms. Subsequently, data reduction and calibration were performed using the HEXRD package[45].

Through an examination of the azimuthally sectioned diffraction images at 15° intervals, it was established that the as-printed Ti-6Al-4V exhibited a larger variation in peak positions (q ($Å^{-1}$)) with azimuth compared to the post-annealed Ti-6Al-4V; however, both variations were marginal (Supplementary Fig. 3). The calibrated diffraction images were azimuthally integrated into intensity profiles. The split Pseudo–Voigt function was employed to fit individual peak profiles of each lattice plane, yielding fitting residuals with an R-squared value over 99%. This process provided peak positions, FWHM, and intensities of profiles. The fitted parameters were monitored in real-time, and a moving average was employed to find the trend of parameter changes. By monitoring changes in lattice spacing over time, the temperature was estimated based on the assumption that the thermal expansion behavior follows the coefficients of thermal expansion (CTE). The method reported in our previous works[9,11] and the CTE data calculated from the reported lattice expansion results were employed[35]. While the estimation is subject to uncertainty from mechanical strain and slight temperature gradients that may exist within the region measured by 50 × 30 μm^2 x-ray beam, it exhibits a high degree of reliability, particularly at elevated temperatures, and tends to offer a generally reasonable range of temperature values[46]. The estimated temperatures were employed to adjust the observed intensity of the diffraction profiles, thereby excluding the influence of thermal vibrations of atoms. This adjustment was achieved by utilizing a general relation with the Debye–Waller effect[32,38]. To approximate the temperature effect in the current study, an averaged Debye characteristic temperature for α-titanium from previous reports was utilized[47,48].

Data availability

The datasets generated during the current study are available from the corresponding author upon reasonable request.

Received: 19 September 2023; Accepted: 4 April 2024;
Published online: 23 April 2024

References

1. Liu, S. & Shin, Y. C. Additive manufacturing of Ti6Al4V alloy: a review. *Mater. Des.* **164**, 107552 (2019).
2. Promoppatum, P. & Rollett, A. D. Influence of material constitutive models on thermomechanical behaviors in the laser powder bed fusion of Ti-6Al-4V. *Addit. Manuf.* **37**, 101680 (2021).
3. Wu, Z. et al. Study of printability and porosity formation in laser powder bed fusion built hydride-dehydride (HDH) Ti-6Al-4V. *Addit. Manuf.* **47**, 102323 (2021).
4. Yu, H. et al. Study on transformation mechanism and kinetics of α' martensite in TC4 alloy isothermal aging process. *Crystals* **10**, 229 (2020).
5. Gil Mur, F. X., Rodríguez, D. & Planell, J. A. Influence of tempering temperature and time on the α'-Ti-6Al-4V martensite. *J. Alloy. Compd.* **234**, 287–289 (1996).
6. Zeng, L. & Bieler, T. R. Effects of working, heat treatment, and aging on microstructural evolution and crystallographic texture of α, α', α'' and β phases in Ti–6Al–4V wire. *Mater. Sci. Eng.: A* **392**, 403–414 (2005).
7. Kaschel, F. R. et al. Mechanism of stress relaxation and phase transformation in additively manufactured Ti-6Al-4V via in situ high temperature XRD and TEM analyses. *Acta Mater.* **188**, 720–732 (2020).

8. Yang, J. et al. Formation and control of martensite in Ti-6Al-4V alloy produced by selective laser melting. *Mater. Des.* **108**, 308–318 (2016).
9. Oh, S. A. et al. High speed synchrotron X-ray diffraction experiments resolve microstructure and phase transformation in laser processed Ti-6Al-4V. *Mater. Res Lett.* **9**, 429–436 (2021).
10. Tan, X. et al. Revealing martensitic transformation and α/β interface evolution in electron beam melting three-dimensional-printed Ti-6Al-4V. *Sci. Rep.* **6**, 26039 (2016).
11. Oh, S. A. et al. Microscale observation via high-speed X-ray diffraction of alloy 718 during in situ laser melting. *JOM* **73**, 212–222 (2020).
12. Zhang, D. et al. Effect of heat treatment on the tensile behavior of selective laser melted Ti-6Al-4V by in situ X-ray characterization. *Acta Mater.* **189**, 93–104 (2020).
13. Sandvik, B. P. J. & Wayman, C. M. Characteristics of lath martensite: part III. Some theoretical considerations. *Metall. Trans. A* **14**, 835–844 (1983).
14. Kaya, M. Ş., Ece, R. E., Keles, O., Qader, A. & Yilbas, B. S. Effect of post processes on mechanical properties of 3D printed Ti6Al4V gears. *J. Mater. Eng. Perform.* **31**, 6300–6309 (2022).
15. Colombo-Pulgarín, J. C. et al. Beta titanium alloys processed by laser powder bed fusion: a review. *J. Mater. Eng. Perform.* **30**, 6365–6388 (2021).
16. Ter Haar, G. M. & Becker, T. H. Selective laser melting produced Ti-6Al-4V: post-process heat treatments to achieve superior tensile properties. *Materials* **11**, 146 (2018).
17. Qiu, C., Adkins, N. J. E. & Attallah, M. M. Microstructure and tensile properties of selectively laser-melted and of HIPed laser-melted Ti–6Al–4V. *Mater. Sci. Eng.: A* **578**, 230–239 (2013).
18. Sofinowski, K. et al. In situ characterization of a high work hardening Ti-6Al-4V prepared by electron beam melting. *Acta Mater.* **179**, 224–236 (2019).
19. Vilaro, T., Colin, C. & Bartout, J. D. As-fabricated and heat-treated microstructures of the Ti-6Al-4V alloy processed by selective laser melting. *Metall. Mater. Trans. A* **42**, 3190–3199 (2011).
20. Vrancken, B., Thijs, L., Kruth, J.-P. & Van Humbeeck, J. Heat treatment of Ti6Al4V produced by selective laser melting: microstructure and mechanical properties. *J. Alloy. Compd.* **541**, 177–185 (2012).
21. Motyka, M. Martensite formation and decomposition during traditional and AM processing of two-phase titanium alloys—an overview. *Metals* **11**, 481 (2021).
22. Saha, D. C., Biro, E., Gerlich, A. P. & Zhou, Y. Martensite tempering kinetics: effects of dislocation density and heating rates. *Mater. Charact.* **168**, 110564 (2020).
23. Sallica-Leva, E., Caram, R., Jardini, A. L. & Fogagnolo, J. B. Ductility improvement due to martensite α' decomposition in porous Ti–6Al–4V parts produced by selective laser melting for orthopedic implants. *J. Mech. Behav. Biomed. Mater.* **54**, 149–158 (2016).
24. Bylica, A. & Sieniawski, J. *Tytan i Jego Stopy* (Państwowe Wydawnictwo Naukowe, 1985).
25. Ji, X. et al. Phase transformation behaviors and dislocation evolutions of an additively manufactured Ti-6Al-4V alloy under annealing treatment. *Metats* **13**, 1061 (2023).
26. Wang, H. et al. Formation of a transition V-rich structure during the α' to α + β phase transformation process in additively manufactured Ti-6Al-4 V. *Acta Mater.* **235**, 118104 (2022).
27. Brown, D. W. et al. Evolution of the microstructure of laser powder bed fusion Ti-6Al-4V during post-build heat treatment. *Metall. Mater. Trans. A* **52**, 5165–5181 (2021).
28. Xu, W., Lui, E. W., Pateras, A., Qian, M. & Brandt, M. In situ tailoring microstructure in additively manufactured Ti-6Al-4V for superior mechanical performance. *Acta Mater.* **125**, 390–400 (2017).
29. Muiruri, A., Maringa, M. & du Preez, W. Evaluation of dislocation densities in various microstructures of additively manufactured Ti6Al4V (Eli) by the method of X-ray diffraction. *Materials* **13**, 5355 (2020).
30. Sato, K., Matsumoto, H., Kodaira, K., Konno, T. J. & Chiba, A. Phase transformation and age-hardening of hexagonal α' martensite in Ti–12mass%V–2mass%Al alloys studied by transmission electron microscopy. *J. Alloy. Compd.* **506**, 607–614 (2010).
31. Couchet, C. et al. Recovery of severely deformed ferrite studied by in situ high energy X-ray diffraction. *Mater. Charact.* **179**, 111378 (2021).
32. Ivanov, I. V., Emurlaev, K. I., Lazurenko, D. V., Stark, A. & Bataev, I. A. Rearrangements of dislocations during continuous heating of deformed β-TiNb alloy observed by in-situ synchrotron X-ray diffraction. *Mater. Charact.* **166**, 110403 (2020).
33. Yonemura, M. et al. Fine microstructure formation in steel under ultrafast heating. *Sci. Rep.* **9**, 11241 (2019).
34. Hou, Z., Babu, R. P., Hedström, P. & Odqvist, J. Microstructure evolution during tempering of martensitic Fe–C–Cr alloys at 700 °C. *J. Mater. Sci.* **53**, 6939–6950 (2018).
35. Elmer, J. W., Palmer, T. A., Babu, S. S. & Specht, E. D. In situ observations of lattice expansion and transformation rates of α and β phases in Ti–6Al–4V. *Mater. Sci. Engin. A* **391**, 104–113 (2005).
36. Lim, R. E. et al. Grain-resolved temperature-dependent anisotropy in hexagonal Ti-7Al revealed by synchrotron X-ray diffraction. *Mater. Charact.* **174**, 110943 (2021).
37. Mishin, Y. & Herzig, Chr. Diffusion in the Ti–Al system. *Acta Mater.* **48**, 589–623 (2000).
38. Cullity, B. D. & Stock, S. R. *Elements of X-Ray Diffraction,* Third Edition. (Prentice-Hall, 2001).
39. Andersson, J.-O., Helander, T., Höglund, L., Shi, P. & Sundman, B. Thermo-Calc & DICTRA, computational tools for materials science. *Calphad* **26**, 273–312 (2002).
40. Yamanaka, K. et al. Quantifying the dislocation structures of additively manufactured Ti–6Al–4V alloys using X-ray diffraction line profile analysis. *Addit. Manuf.* **37**, 101678 (2021).
41. Matsuyama, S. & Galindo-Nava, E. I. A unified model for plasticity in ferritic, martensitic and dual-phase steels. *Metals* **10**, 1–33 (2020).
42. Wei, M. & Wen, Y. Martensitic transformation from β to α' and α″ phases in Ti–V alloys: a first-principles study. *J. Mater. Res* **32**, 3183–3190 (2017).
43. Ming, L.-c, Manghnani, M. H. & Katahara, K. W. Phase transformations in the Ti-V system under high pressure up to 25 GPa. *Acta Metall.* **29**, 479–485 (1981).
44. Johnson, N. S. et al. The roles of kinematic constraint and diffusion in non-equilibrium solid state phase transformations of Ti-6Al-4V. *Appl. Phys. Lett.* **120**, 171901 (2022).
45. Bernier, J. et al. HEXRD/hexrd: release 0.9.3. *Zenodo* https://doi.org/10.5281/zenodo.8033940 (2023).
46. Lim, R. E. et al. Combining synchrotron X-ray diffraction, mechanistic modeling and machine learning for in situ subsurface temperature quantification during laser melting. *J. Appl. Crystallogr.* **56**, 1131–1143 (2023).
47. Chen, Q. & Sundman, B. Calculation of debye temperature for crystalline structures—a case study on Ti, Zr, and Hf. *Acta Mater.* **49**, 947–961 (2001).
48. Argaman, U., Eidelstein, E., Levy, O. & Makov, G. Thermodynamic properties of titanium from ab initio calculations. *Mater. Res. Express* **2**, 016505 (2015).

Acknowledgements

This work was supported by the National Nuclear Security Administration under grant number DE-NA0003915. This research used resources of the Advanced Photon Source, a U.S. Department of Energy (DOE) Office of Science User Facility operated for the DOE Office of Science by Argonne National Laboratory under Contract No. DE-AC02-06CH11357. The apparatus for rapid laser heating was originally developed by Prof. Tao Sun

(Northwestern Univ.). The authors acknowledge use of the Materials Characterization Facility (MCF) at Carnegie Mellon University, supported by grant MCF-677785.

Author contributions

S.O.: conceived the study, planned/performed experiments, data analysis, and wrote the original draft. J.A.: conceived the study and performed experiments. N.L.: prepared AM-printed samples. A.C.: designed and planned experiments. A.B.: helped with data analysis and interpretation. A.R.: conceived and supervised the study and acquired funding. All authors contributed to the review and edit the draft.

Competing interests

The authors declare no competing interests.

Additional information

Supplementary information The online version contains supplementary material available at https://doi.org/10.1038/s43246-024-00492-6.

Correspondence and requests for materials should be addressed to Seunghee A. Oh or Anthony D. Rollett.

Peer review information *Communications Materials* thanks Mert Celikin, Yuanfei Han and the other, anonymous, reviewer(s) for their contribution to the peer review of this work. Primary Handling Editors: Xiaoyan Li and John Plummer. A peer review file is available.